# Time-Course Imaging of Rat Embryos *In Utero* with Magnetic Resonance Microscopy

Bradley R. Smith, Mark D. Shattuck, Laurence W. Hedlund, G. Allan Johnson

**Magnetic resonance (MR) microscopy was used to noninvasively investigate the development of live rat embryos *in utero*. The difficulty in making sequential observations of a developing mammalian embryo has frustrated developmental biologists for many years. Most current technologies analyze normal and abnormal development by observing end point phenotypes (in fixed specimens) rather than investigating the live embryo. MR microscopy was adapted to allow rat litters to be scanned three times each (at 1- to 3-day intervals) and has produced images of live developing embryos. It was demonstrated that repeated anesthesia and imaging protocols produced no gross malformations in the rat pups that were subsequently delivered and observed. Three-dimensional projection encoding with phase rewinders produced isotropic ($256^3$) image data sets in about 30 minutes with excellent tissue contrast arising from steady-state effects in the amniotic fluid.**

**Key words: *in utero* imaging; projection encoding; live rat embryo; fetus.**

## INTRODUCTION

Developmental biologists are producing new animal models at an unprecedented pace with recently discovered gene manipulation techniques. Tools that can analyze these genetically altered embryos are desperately needed (1, 2). In many vertebrate and invertebrate animals (the chick, fish, sea urchin, fruit fly), easy access to the embryo facilitates direct analysis of development. However, development of the mammalian embryo is difficult to observe noninvasively because of its position deep within the uterus, where it is surrounded by the placenta and extraembryonic membranes. Consequently, normal and abnormal developmental events in mammals have been deduced from observations of multiple embryos sacrificed at different stages of growth. Large numbers of animals must be studied to achieve statistically reliable evidence that a condition observed early in development will lead to a phenotype observed later.

The present study tested magnetic resonance (MR) microscopy as a noninvasive, high-resolution imaging technique for analyzing mammalian embryos and fetuses *in utero*. It also tested our ability to make repeated observations of maturing rat embryo litters without disrupting normal development. The techniques described here have the potential to accelerate the analysis of the numerous genetically engineered mammals being produced.

MR microscopy has been used for several years now to investigate developmental questions in live embryo models (3–5) as well as fixed embryos and fetuses (6–9). The major challenges facing MRI of the live embryo include motion, limited signal, low inherent contrast, and maternal physiological instability during image acquisition. The types of motion that are detrimental to MRI of embryos include embryo growth, diffusion at the molecular level, maternal gut and uterine motility, maternal breathing, embryonic movement, maternal cardiac motion and blood flow, and embryonic cardiac motion and blood flow. These sources of motion must be effectively compensated or accommodated to obtain artifact-free images. Imaging coils must match the small specimen size to maintain good signal-to -noise ratios and the coil design must also allow the mother to be well monitored and stabilized during the imaging sequences to ensure viable and healthy offspring. Pulse sequences exploiting contrast properties intrinsic to embryonic tissues must be used because the minimally differentiated tissues of embryos would otherwise produce very low contrast images. All of these factors must be carefully balanced to obtain data that are meaningful to the developmental biologist.

## METHODS

### Animal Support

Animal procedures were approved by the Duke University Institutional Animal Care and Use Committee. Pregnant female Sprague-Dawley rats ($N$ = 10, 250 to 300 g, Charles River Laboratories, Wilmington, MA) were anesthetized with methohexital sodium (intraperitoneal, 40 mg/kg, Brevital, Eli Lily Co. Indianapolis, IN) and perorally intubated with an 18-gauge intracatheter (Baxter Healthcare Corporation, Deerfield, IL). They were also given atropine sulfate. Anesthesia was maintained during imaging with a mixture of isoflurane (1.5–2.5%, Aerrane, Ohmeda Caribe, Inc., Guayama, Puerto Rico) and air using an MRI-compatible pressure ventilator. The pregnant female was typically under anesthesia for 2–3 hours to allow for animal setup time and for testing several pulse sequences and coil sizes. ECG was recorded continuously from pediatric electrodes taped to the foot pads, an esophageal-thermistor monitored temperature, and a solid-state pressure transducer on the breathing-valve monitored airway pressure. Physiological signals were processed (Coulbourn Instruments, Allentown, PA) and displayed on a Macintosh computer using

**MRM 39:673–677 (1998)**

From the Department of Radiology, Duke University Medical Center, Durham, North Carolina (B.R.S., L.W.H., G.A.J.); and the University of Texas Physics Department and Center for Nonlinear Dynamics, Austin, Texas.

Address correspondence to: Bradley R. Smith, Ph.D., Box 3302, Department of Radiology, Duke University Medical Center, Durham, NC 27710.

Received April 2, 1997; revised October 13, 1997; accepted October 13, 1997.

This work was supported by Grant P41 RRO5959 from the National Institutes of Health.

0740-3194/98 $3.00

an A/D board (MIO-16, National Instruments, Austin, TX) and LabVIEW software (National Instruments). A feedback loop in the physiological monitor software automatically controlled body temperature (36.7 ± 0.3°C) by controlling the flow of heated air through the bore of the magnet (10).

Pregnant rats were divided into two groups: controls , nonimaged and nonanesthetized ($n = 4$); and imaged ($n = 6$). Of the rats in the imaged group, one died during imaging due to ventilation failure and a second died 3 days after imaging from unknown causes. Of the remaining four imaged rats, three rats were imaged at three times (ages ranging from embryonic (E) day 11 to E20, E1 being the morning after a plug confirmed the overnight mating) with at least 2 days of rest between imaging sessions and one rat was imaged once. The eight rats completing the study came to term, and each litter was weighed as a group for 18 days postpartum. At parturition, each pup was examined individually for any signs of gross abnormality. At the completion of the 18 days, the adults were sacrificed by anesthetic overdose and the uterine horns were examined for number of implantation sites.

### MRI

All work was performed at 2.0 T in a 30-cm horizontal-bore magnet configured for MR microscopy. Shielded coils provided 18 G/cm gradients with rise times of <200 $\mu$s. The system was controlled by a GE Signa console (General Electric Medical Systems, Milwaukee, WI) adapted for operation at 85 MHz through the use of an intermediate frequency conversion stage.

Two RF coils, 50- and 25-mm surface coils, were etched onto microwave substrate with an additional loop etched on the periphery of the coils to provide balanced inductive coupling. Three-dimensional projection encoding was used as described more fully elsewhere (11, 12), with an effective TE = 3.5 ms and TR = 8 ms, with phase rewinders, and $\alpha = 10°$ in the center of the images.

Fourier space was sampled isotropically over a spherical FOV. Because we were encoding the FID, the effective TE was the time between the center of the nonselective RF excitation and the first point sampled. This effective TE could be made as short as 210 $\mu$s. For these studies, we chose a longer effective TE of 3.5 ms, which is the period corresponding to the chemical shift difference between fat and water. This minimized off-resonance artifacts. To summarize, a total of 205,780 projections were acquired at TR = 8 ms for a total acquisition time of 27.4 minutes. The acquisition bandwidth was 32 kHz for a total readout time per view of 4 ms. The first point of each FID was acquired 3.5 ms after the end of the $\alpha$ pulse to ensure that fat and water were out of phase at the center of $k$-space. The radial trajectories were regridded onto a Cartesian array that was Fourier-transformed and displayed as a magnitude image.

### Image Visualization

Reconstructed images were volume-rendered and reformatted using VoxelView ULTRA 2.5 software (Vital Images, Fairfield, IA) on a Reality Engine$^2$ Workstation (Silicon Graphics, Mountain View, CA) to produce single-slice images in various planes and volume-rendered slabs of various thicknesses.

## RESULTS

We successfully acquired three-dimensional image arrays of live rat embryos without producing gross abnormalities in any of the newborn pups. These images, with high contrast and little motion artifact, allowed us to observe important anatomical landmarks within the conceptus at three different ages during a single pregnancy. The anatomical detail available from the three-dimensional image arrays taken from a single litter imaged at E13, E16, and again at E20 is depicted in Fig. 1. The following structures are readily identified at E13: the maternal uterine wall, placenta, amniotic fluid, umbilical stalk, limb buds, dorsal neural tube, telencephalic vesicle, and the heart (Fig. 2). At E16, the following anatomy is observed: the maternal uterine wall, placenta, amniotic fluid, umbilical stalk, limbs, dorsal neural tube, telencephalic vesicle, third ventricle, fourth ventricle, forebrain, midbrain, hindbrain, diencephalon (thalamus), cardinal veins, heart, and aorta (Fig. 2). At E20, the following are observed: the maternal uterine wall, placenta, amniotic fluid, umbilical stalk, limbs, cervical spinal cord, cardinal veins, sinus venosus, right atrium, heart, and liver.

The number of embryos that could be contained within the FOV diminished between E13 and E20 because of fetal growth. About eight embryos could be observed at E13, six at E16, and only four at E20. Furthermore, it was more difficult to identify structures within the embryos or to distinguish placental from uterine tissue in the oldest animals because of the relative decrease in the amount of very high-signal amniotic fluid surrounding the low-signal fetal tissues (see Fig. 1, E20).

The 50-mm surface coil provided adequate signal from approximately two-thirds of the pregnant female's lower abdomen and pelvis until E17, when only approximately one-half of the region containing embryos was detected. There was remarkably little evidence of motion artifact produced by the mother or the embryos until about E19, when gross fetal movement degraded the images. It is noteworthy that the embryonic heartbeat did not disturb the image quality at the younger ages, although it might have contributed to some of the motion artifact detected in the oldest embryos. Maternal blood flow, gut mobility, and breathing did not seem to degrade the image quality at any age. The images had particularly high contrast between the amniotic fluid and all other maternal and fetal tissues when phase rewinders were used but lacked this contrast without phase rewinders (Fig. 3). The fetal cerebrospinal fluid also provided very high signal in contrast to the surrounding fetal tissue. The contrast within fetal tissues, however, was low at all stages studied.

The imaging protocol seems to have had minimal impact on the pregnant rats and allowed the birth of pups without gross abnormalities. The imaged rats tended to have slightly lower body weight immediately postpartum

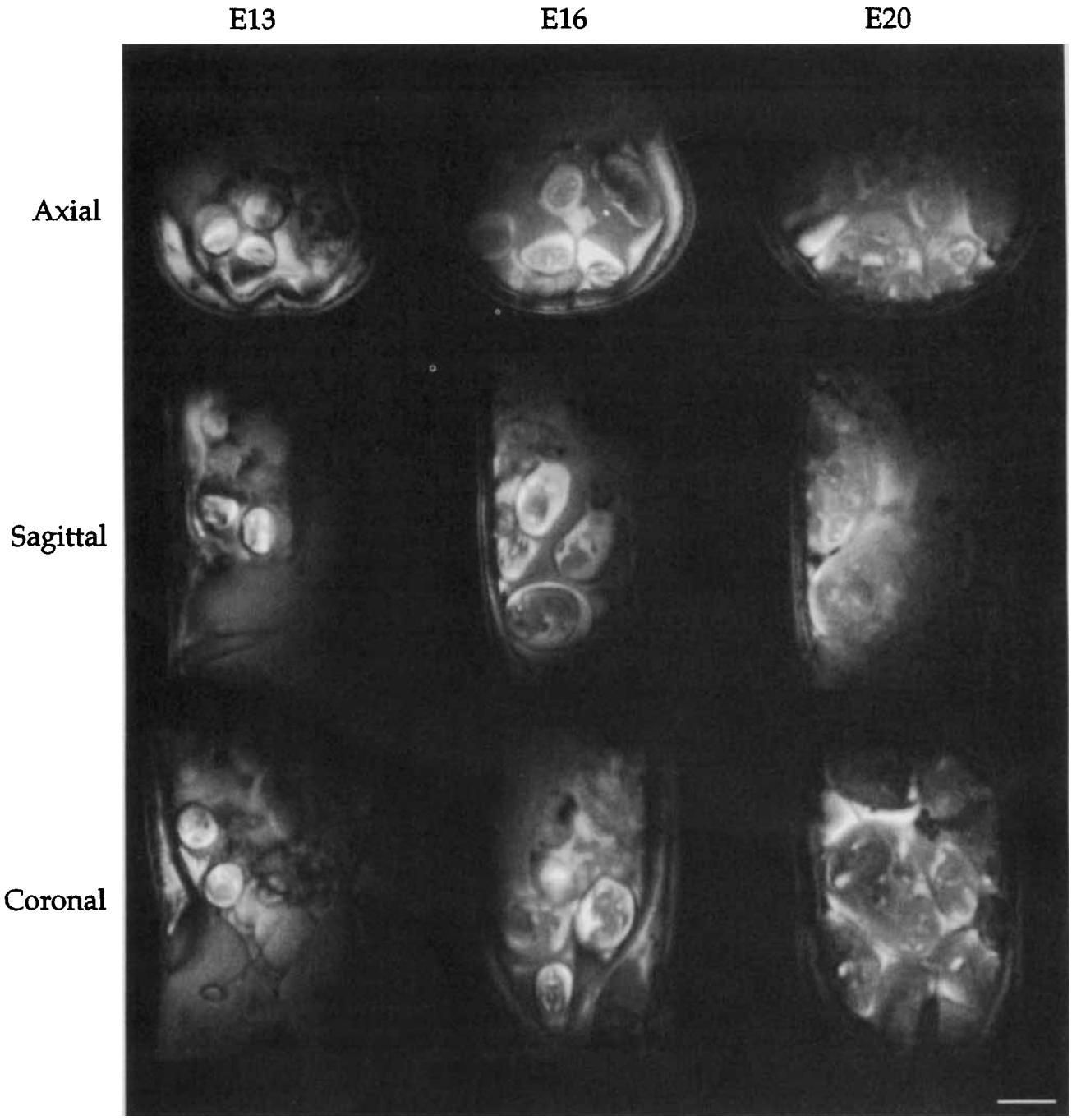


FIG. 1. Axial, sagittal, and coronal images from an *in utero*, time-course study of a single rat litter at embryonic days 13, 16, and 20. Image resolution and tissue contrast is sufficient to observe changes in important vascular and neural embryonic structures (anatomic structures are labeled in Fig. 2). These reformatted images have each been volume-rendered from four slices out of the three-dimensional data sets. The voxel dimensions for each single slice was 195 × 195 × 195 microns. Bar = 10 mm.

compared to the nonimaged group, which may be due to reduced food intake after the days of imaging (data not shown). At birth, each pup was examined and no gross abnormalities were found in either the imaged group or the controls. All pups survived during the postpartum examination period of 18 days. Fig. 4 is the daily average pup weight for 18 postpartum days. We counted uterine implantation sites of all females to account for possible spontaneous or imaging-induced abortions. The controls had an average of 14.3 implantation sites and 12.8 pups per litter, whereas the imaged group had an average of 13.5 implantation sites and 13 pups per litter. Although we did not study sufficient animals to provide statistical analysis, these results suggest that the imaging procedure did not generate more resorptions or spontaneous abortions than occurred in the control group and that the pups were not adversely affected by the imaging procedure. This is important in light of our finding no previous

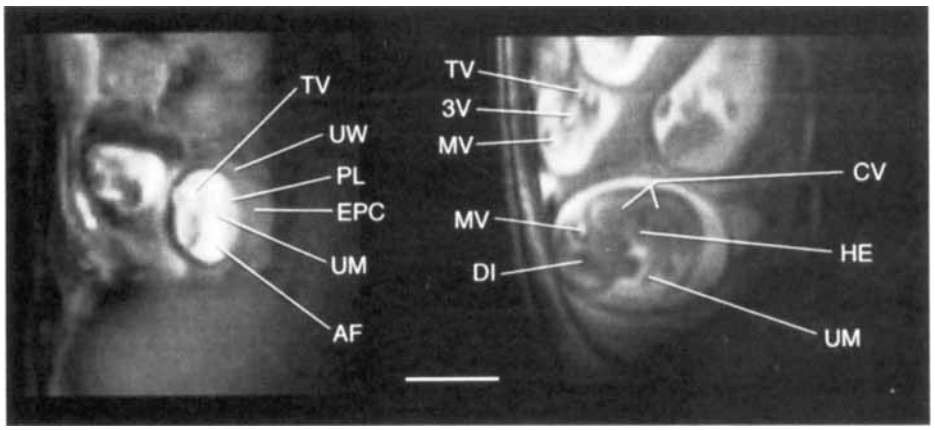


FIG. 2. Sagittal images from an *in utero* study of a rat litter at embryonic days 13 (a) and 16 (b). AF = amniotic fluid, CV = cardinal veins, DI = diencephalon, EPC = ectoplacental cone, HE = heart, MV = mesencephalic vesicle, PL = placenta, TV = telencephalic vesicle, UM = umbilicas, UW = uterine wall, 3V = third ventricle, Bar = 10 mm.

reports on the consequence of multiple maternal anesthetic episodes to the embryo.

## DISCUSSION

Our ability to resolve specific structures in the live embryo is constrained by both signal contrast and spatial resolution. As Fig. 1 clearly demonstrates, there is significant contrast between the soft tissues and the surrounding amniotic fluid. The long $T_2$ of the amniotic fluid becomes an *in vivo* contrast agent because the ratio of $T_1/T_2$ is significantly different from any other tissues. This is particularly apparent when phase rewinders are used because these will maintain the steady state. Without rewinders, contrast is determined primarily by TR and the RF excitation angle ($\alpha$). When rewinders are applied, spin phase is maintained between successive views and the contrast becomes much more dependent on $T_2$.

Spatial resolution is limited primarily by motion in these studies. Motion as expressed by diffusion at the molecular level and embryo growth did not produce imaging artifacts in our studies. However, respiratory motion, cardiac motion of the mother and the individual embryos, peristaltic motion of the mother, and motion of the individual embryo did need to be accommodated. The pulse sequence used in this study has a great deal of immunity to these motion artifacts because (a) the effective echo is so short, (b) the center of *k*-space is highly oversampled, and (c) the radial trajectories place motion artifacts away from the center of the image. The limited range of the surface coils was exploited in both transmit and receive to restrict the initial excited volume and constrain the FOV for reconstruction. This permitted the use of nonselective RF pulses, which, in turn, allowed us to use short TRs. The FID was sampled with increasing spacing along the radial axis of Fourier space, and the spatial encoding gradients were ramped to their full scale, typically accomplished in <600 $\mu$s. Ramping caused the radial sampling density along each view to increase toward the center of Fourier space (low spatial frequencies) and added to the high azimuthal sampling density, which is inherent in radial sampling. Averaging of the high density of samples in the low spatial frequencies reduced motion artifacts significantly. Furthermore, motion artifacts were generally reconstructed outside the central part of the image because of the unique properties of radial sampling (13).

We anticipate improved imaging of live rodent embryos *in utero* with refinements in coil design, pulse sequence execution, and animal handling (i.e., scan-synchronous ventilation) (12). The use of implanted coils would have the signal-to-noise advantages associated with a higher filling

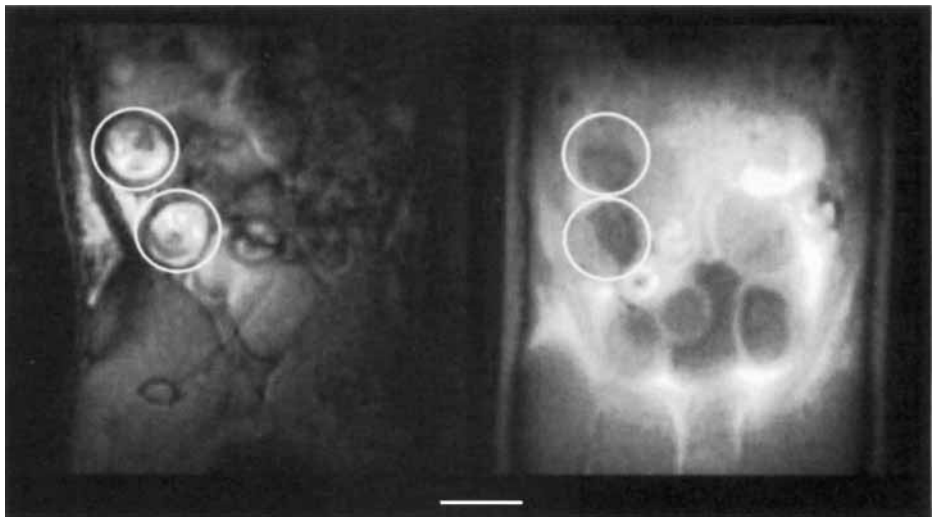


FIG. 3. Coronal views of two different rat litters *in utero* on embryonic day 13. The use of a phase-rewinding gradient generates high contrast between the amniotic fluid and tissues of the conceptus (a), whereas the same pulse sequence without the rewinder generates an image with very little contrast between the amniotic fluid and conceptus (b). A conceptus (embryo plus extraembryonic membranes) is shown within each circle. Bar = 8 mm.

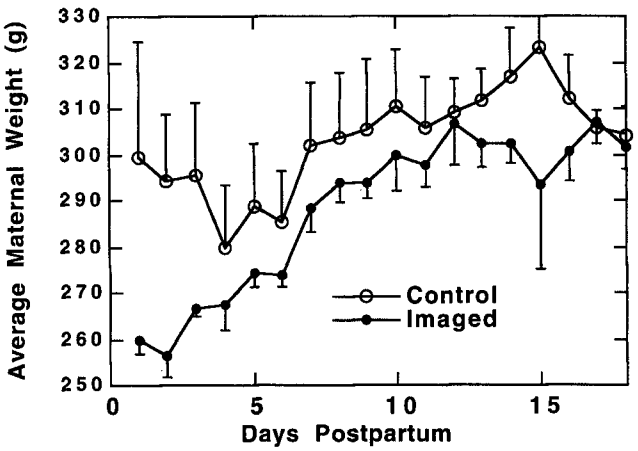


FIG. 4. The average weight of newborn pups from mothers that had been imaged during pregnancy starts moderately lower than control pups, but by day 2, there is no difference ($n$ = 51 pups born in four control litters and 44 pups born in four imaged litters, $x \pm$ SEM).

factor. Such a coil could be placed very close to or even around the developing embryo. However, the surgery involved with the coil placement and its presence so close to the embryo could disrupt normal development and spoil the observations being made.

The explosion of genetically manipulated embryos, the lack of effective tools to analyze them, and the preliminary success with MR microscopy to study fixed and live embryos suggest that these efforts to refine high-resolution MRI will produce an important tool for developmental biologists.

## ACKNOWLEDGMENTS

The authors thank Daniel Turnbull for motivating this work and for reviewing the image data and Elaine Fitzsimons for editing the manuscript.

## REFERENCES

1. A. Nagy, J. Rossant, Targeted mutagenesis: analysis of phenotype without germ line transmission. *J. Clin. Invest.* **97,** 1360–1365 (1996).
2. K. Chien, Genes and physiology: molecular physiology in genetically engineered animals. *J. Clin. Invest.* **97**, 901–909 (1996).
3. S. N. Bone, G. A. Johnson, M. B. Thompson, Three-dimensional magnetic resonance microscopy of the developing chick embryo. *Invest. Radiol.* **21,** 782–787 (1986).
4. R. E. Jacobs, S. E. Fraser, Magnetic resonance microscopy of embryonic cell lineages and movements. *Science* **256,** 681–684 (1994).
5. B. Smith, Magnetic resonance microscopy with cardiovascular applications. *Trends Cardiovasc. Med.* **6,** 247–254 (1996).
6. B. R. Smith, E. L. Effmann, G. A. Johnson, MR microscopy —chick embryo vasculature. *J. Magn. Reson. Imaging* **2,** 237–240 (1992).
7. S. Kornguth, E. Bersu, M. Anderson, J. Markley, Correlation of increased levels of class I MHC H-2K in the placenta of murine trisomy 16 conceptuses with structural abnormalities revealed by magnetic resonance microscopy. *Teratology* **45**, 383–391 (1992).
8. B. R. Smith, G. A. Johnson, E. V. Groman, E. Linney, Magnetic resonance microscopy of mouse embryos. *Proc. Natl. Acad. Sci. U S A* **91,** 3530–3533 (1994).
9. B. Smith, E. Linney, D. Huff, G. Johnson, Magnetic resonance microscopy of embryos. *Comput. Med. Imaging Graph.* **20,** 483–490 (1996).
10. H. Qui, G. Cofer, L. W. Hedlund, G. A. Johnson, Automated feedback control of body temperature for small animal studies with MR microscopy. *IEEE Trans. Biomed. Eng.* **44,** 1107–1113 (1997).
11. S. L. Gewalt, G. H. Glover, J. R. MacFall, L. W. Hedlund, G. A. Johnson, MR microscopy of the rat lung using projection reconstruction. *Magn. Reson. Med.* **29,** 99–106 (1993).
12. M. D. Shattuck, G. P. Cofer, G. H. Glover, L. W. Hedlund, G. A. Johnson, Three-dimensional projection microscopy of the lung, *in* "Proc., SMR, 4th Annual Meeting, New York, 1996," p. 18.
13. G. H. Glover, J. M. Pauly, Projection reconstruction techniques for suppression of motion artifacts. *Magn. Reson. Med.* **28,** 275–289 (1992).